

# SGDR: Semantic-guided Disentangled Representation for Unsupervised Cross-modality Medical Image Segmentation

Shuai Wang, Rui Li  
Tsinghua University

s-wang20@mails.tsinghua.edu.cn, leerui@tsinghua.edu.cn

## Abstract

*Disentangled representation is a powerful technique to tackle domain shift problem in medical image analysis in unsupervised domain adaptation setting. However, previous methods only focus on exacting domain-invariant feature and ignore whether exacted feature is meaningful for downstream tasks. We propose a novel framework, called semantic-guided disentangled representation (SGDR), an effective method to exact semantically meaningful feature for segmentation task to improve performance of cross modality medical image segmentation in unsupervised domain adaptation setting. To exact the meaningful domain-invariant features of different modality, we introduce a content discriminator to force the content representation to be embedded to the same space and a feature discriminator to exact the meaningful representation. We also use pixel-level annotations to guide the encoder to learn features that are meaningful for segmentation task. We validated our method on two public datasets and experiment results show that our approach outperforms the state of the art methods on two evaluation metrics by a significant margin.*

## 1. Introduction

Recently, deep learning methods have achieved great success in medical image analysis [13], such as segmentation [19, 26, 31], detection [32, 37, 41] and so on. There is a common assumption that training and test images are sampled from the sample distribution identically, *i.e.* independently identically distribution. However, in real-world scene, especially in medical image analysis, due to different imaging principles and acquisition parameters, a large domain gap between training data and test data usually occurs, as shown in Fig. 1. The large domain gap reduces the performance on test set and limits the application of deep learning model.

To reduce the domain gap and improve the performance, fine-tuning the model pre-trained on source domain with la-

beled data is a trivial way. But it requires pixel-level annotations on the target domain, which is time-consuming and expensive. Unsupervised domain adaptation (UDA) has attracted the attention in medical image analysis community [5, 9, 12, 22, 25, 29, 30]. In UDA setting, given labeled data from source domain and unlabeled data from target domain, our goal is to learn a model can segment the target domain in an unsupervised training manner.

For the existing UDA methods, there are two categories: distance-based methods [3, 27, 36, 38, 39] and adversarial training methods [7, 21, 22, 29, 30, 40]. Disentangled representation is often used in adversarial training methods, which is a powerful technique to exact the domain-invariant features and domain-specific features between source domain and target domain. However, previous methods only focus on exacting features and do not consider whether exacted features are semantically meaningful for special task, such as segmentation, which leads to sub-optimal results.

By contrast, we propose a novel method to exact more meaningful features for our segmentation task. First, we disentangle images of source domain and target domain onto content space and style space. Content space includes domain-invariant information, such as anatomical structure and style space includes domain specific information, such as modality or contrast. Generator learns to perform image-to-image translation combing the content features and style information. Specially, we use a content discriminator to enforce the encoder exact the domain-invariant features between source domain and target domain. To learn more meaningful and semantic-related features, we introduce a feature discriminator and auxiliary segmentation loss. We use cross cycle consistency loss to help our model can handle unpaired data. Our model can be trained end to end with adversarial training.

Our contribution could be summarized as follows. First, we present a novel unsupervised domain adaptation framework via disentangled representation. Second, we introduce semantic-guided strategy to make exacted features more suitable for downstream tasks, such as semantic segmentation. Third, we conduct extensive experiments in the three

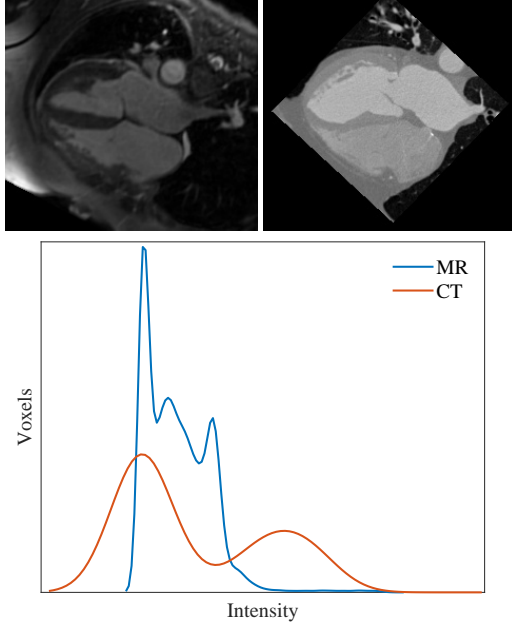


Figure 1. Illustration of domain shift. Examples of MR and CT images from different subjects are shown in the first row. The second is intensity distribution of examples. In addition to the difference in gray distribution between MR and CT images, there is also an offset of anatomical structure

cardiac segmentation tasks and experiment results show that our method consistently improves the performance in unsupervised domain adaptation setting and outperforms the state of the art approaches.

## 2. Related Work

This work is mainly related to two areas: domain adaptation and disentangled representation.

### 2.1. Domain Adaptation

Domain adaptation is a potential technology for tackling domain shift problem in medical image analysis. Previous domain adaptation methods can be divided into two categories: a) minimizing the distance metrics to align the data in a common space explicitly. b) adversarial training which reduce the domain gap implicitly based on generative adversarial network [16].

Tzeng *et al.* [36] and Long *et al.* [27] minimized the Maximum Mean Discrepancy (MMD) to reduce the domain discrepancy. Sun [33] proposed COARL, which aligns the second-order statistics of the source domain and target domain. Courty *et al.* [10] proposed a novel method that minimizes the optimal transport loss between the joint source distribution and an estimated target joint distribution. Kang *et al.* [23] proposed pixel-level cycle association to build the connection between source and target pixel pairs, which

is a new perspective for semantic segmentation under unsupervised domain adaptation setting. For medical image segmentation, Wu and Zhang [38] proposed Characteristic Function Distance (CFD) to reduce the domain gap in frequency domain through Fourier Transformation. Chanti [3] proposed a method that learns a shared cross-domain latent space by variational auto-encoder and optimal transport theory.

Generative adversarial network [16] is widely used in image generation and domain adaptation. The main idea is to align the source data and target data on image level or feature level by adversarial training. In unsupervised domain adaptation setting, some methods aim to learn domain-invariant features across domains [12, 14, 22, 34, 35], while other methods aligns the source domain image and target domain image on image level [7, 9, 21] based some image to image networks, such as CycleGAN [42], MUNIT [18] or DRIT [24]. Chen *et al.* [5] presented a novel framework aligns source domain and target domain on both image level and feature level, which achieves the state of the art performance.

### 2.2. Disentangled Representation

Disentangled representation aims to learn domain-invariant feature and domain-specific feature simultaneously from paired [15] or unpaired data [18, 24]. InfoGAN [8] learns disentanglement representation by maximizing the variational upper bound of mutual information between latent variables and data variation. Disentangling multimodal images has been used for liver segmentation with domain adaptation [40]. Bousmils *et al.* [2] explicitly separated domain-invariant features and domain-specific by encouraging orthogonality between shared and specific of each domain. Pei *et al.* [30] introduce zero-loss [1] to enhance the disentanglement for cross-modality cardiac segmentation. However, previous methods only focus on extracting domain-invariant features, and ignore whether the extracted features are meaningful for downstream tasks, such as classification, detection and segmentation. This leads to performance degradation. To tackle this problem, we propose semantic-guided disentangled representation by using pixel-level annotations of source domain and two discriminators to help capturing the meaningful representation.

## 3. Method

An overview of our method is shown in Fig. 2. We first disentangle image of each domain onto two space: domain-invariant space  $\mathcal{C}$  and domain specific space  $\mathcal{S}_X$  and  $\mathcal{S}_Y$  using four encoders. After that, we swap the domain-invariant features of each domain and feed them into generators to get fake images. And we repeat the encoding and generation on the generated fake images. Moreover, we use a content discriminator  $D^c$  to get the domain-invariant fea-

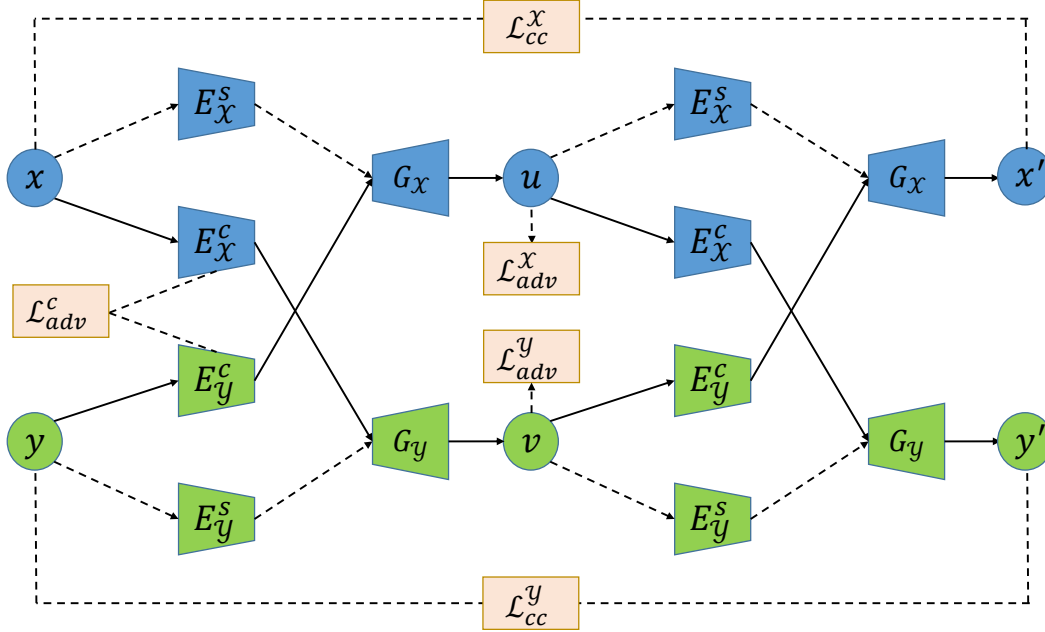


Figure 2. Our framework overview (Sec. 3.2).  $x$  and  $y$  are sampled images from source domain  $\mathcal{X}$  and target domain  $\mathcal{Y}$  respectively.  $\{E_x^c, E_y^c\}$  and  $\{E_x^s, E_y^s\}$  are corresponding content encoders and corresponding style encoders.  $\{G_x, G_y\}$  are image generators.  $u$  and  $v$  are translated images of source domain and target domain.  $x'$  and  $y'$  are cross cycle reconstructed images of  $x$  and  $y$ .

tures. To make exacted features more meaningful and suitable for segmentation tasks, we use semantic-guided representation learning strategy. More details will be discussed in Sec. 3.2. The other parts are organized as follows. We introduce our problem setting, *i.e.* unsupervised domain adaptation for medical image segmentation in Sec. 3.1. The total objective function and implement details could be found in Sec. 3.3 and Sec. 3.4.

### 3.1. Problem Definition

We consider semantic segmentation of unsupervised domain adaptation. Let denote labeled data from source domain as  $\{(x^i, x_{gt}^i) | i = 1, 2, 3 \dots, M\}$  and unlabeled data from target domain as  $\{y^i | i = 1, 2, 3 \dots, N\}$ , respectively, where  $x^i$  and  $y^i$  denote images from source domain and target domain and  $x_{gt}^i$  is pixel-level annotation of  $x^i$ . Our goal is to train a model from labeled data from source domain data and unlabeled data from target domain and the model can segment data from target domain directly.

### 3.2. Semantic-guided Disentangled Representation

Let  $x \in \mathcal{X}$  and  $y \in \mathcal{Y}$  denote unpaired images are sampled from source domain  $\mathcal{X}$  and target domain  $\mathcal{Y}$ . Our method embeds images to content space  $\mathcal{S}_x$  and  $\mathcal{S}_y$ . Content space includes domain-invariant features and style space includes domain specific features. Intuitively, in terms of medical images, the content space include domain-invariant features such as anatomical struc-

ture and the style space includes modal information such as contrast. The content encoder  $E_x^c$  or  $E_y^c$  should exact the shared information between the source domain and target domain, while style encoder  $E_x^s$  or  $E_y^s$  encodes the domain specific information onto  $\mathcal{S}_x$  and  $\mathcal{S}_y$ .

To facilitate the factorization of content and style feature, we use a content discriminator  $D^c$  to make the encoders of source domain and target domain, *i.e.*  $E_x^c$  and  $E_y^c$ , exact the domain-invariant features. The content discriminator  $D^c$  aims to distinguish the content representation from source domain or target domain. The content encoders learn to exact domain invariant features that can't be distinguished by the content discriminator. We formulate this adversarial training process as follows:

$$\mathcal{L}_{adv}^c = \mathbb{E}_x[\log D^c(E_x^c(x)) + \log(1 - D^c(E_x^c(x)))] + \mathbb{E}_y[\log D^c(E_y^c(y)) + \log(1 - D^c(E_y^c(y)))] \quad (1)$$

However, domain-invariant information is not always meaningful for semantic segmentation. Moreover, meaningless information will cause performance degradation. We introduce a feature discriminator and an auxiliary loss function to help the encoder get more meaningful information for segmentation. First, we add a segmentation network  $S_{seg}$  after content encoder, as shown in Fig. 3. We can train content encoder  $E_x^c$  and segmentation network  $S_{seg}$  together with source domain label to make content features more meaningful for segmentation task. The segmentation

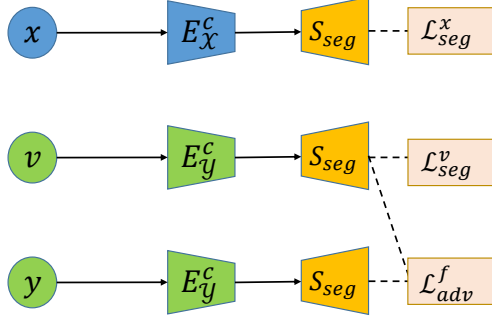


Figure 3. Illustration of our semantic-guided strategy.  $S_{seg}$  is segmentation module to get segmentation prediction. In order to capture meaningful representation from input images, we add segmentation loss to content encoder  $E_{\mathcal{X}}^c$  and segmentation module  $S_{seg}$ . As anatomical structure is similar between the source domain and target domain, we introduce a feature discriminator to force the anatomical structure of target domain to be as close to source domain.

loss is as follows:

$$\mathcal{L}_{seg}^x = Dice(\tilde{x}, x_{gt}) + CE(\tilde{x}, x_{gt}) \quad (2)$$

where  $\tilde{x} = S_{seg}(E_{\mathcal{X}}^c(x))$  is segmentation prediction of source domain.  $Dice$  represents Dice loss and the second term  $CE$  is cross-entropy loss. We also add an auxiliary segmentation loss  $\mathcal{L}_{seg}^v$  to constrain the anatomical shape of fake images as shown in Fig. 3. The segmentation loss is defined as:

$$\mathcal{L}_{seg}^v = Dice(\tilde{v}, x_{gt}) + CE(\tilde{v}, x_{gt}) \quad (3)$$

where  $\tilde{v} = S_{seg}(E_{\mathcal{Y}}^c(v))$ . The total segmentation loss is formulated as follows:

$$\mathcal{L}_{seg} = \mathcal{L}_{seg}^x + \mathcal{L}_{seg}^v \quad (4)$$

In order to improve performance on target domain and exact more meaningful features, we introduce feature adversarial training for content encoders  $E_{\mathcal{Y}}^c$  and segmentation module  $S_{seg}$ , which could be view as semantic-level supervision. It is noted that anatomical structures are similar between source domain and target domain, so the feature discriminator would fail to distinguish segmentation masks from source domain or target domain. The adversarial training loss could be formulated as follows:

$$\mathcal{L}_{adv}^f = \mathbb{E}_v[\log D^f(S_{seg}(E_{\mathcal{Y}}^c(v)))] + \mathbb{E}_y[\log(1 - D^f(S_{seg}(E_{\mathcal{Y}}^c(y))))] \quad (5)$$

where  $D^f$  is a discriminator to distinguish segmentation mask comes from  $y$  or  $v$ .

For style encoding, we follow the common approach in [4, 6, 24] and we set style encoding  $s \in R^8$  assuming its posterior distribution  $q(s|x)$  to be a Gaussian distribution  $\mathcal{N}(0, I)$ . We use Kullback-Leibler (KL) divergence to force  $q(s|x)$  to be close to the normal distribution for training style encoder, the KL loss is formulated as follows:

$$\mathcal{L}_{KL} = D_{KL}(q(s|x)||\mathcal{N}(0, I)) \quad (6)$$

where  $D_{KL}(p||q) = \int p(x) \ln(\frac{p(x)}{q(x)}) dx$ .

After disentangling images to content space and style space, we combine the content feature and style feature into generator  $G_{\mathcal{X}}$  or  $G_{\mathcal{Y}}$  and get a fake image  $u = G_{\mathcal{X}}(E_{\mathcal{Y}}^c(y), E_{\mathcal{X}}^s(x))$  or  $v = G_{\mathcal{Y}}(E_{\mathcal{X}}^c(x), E_{\mathcal{Y}}^s(y))$ .  $u$  has the same anatomical structure with  $y$  and same style with  $x$ , *i.e.*  $u$  and  $x$  should come from the same domain. We use adversarial training to generate more realistic image of source domain or target domain. We denote adversarial training loss as  $\mathcal{L}_{adv}^x$  and  $\mathcal{L}_{adv}^y$ . For  $\mathcal{L}_{adv}^x$  and  $\mathcal{L}_{adv}^y$ , we use a least-square loss [28], which is more stable during training process and generates more realistic images. In particular, for  $\mathcal{L}_{adv}^x$ , we train the  $G_{\mathcal{X}}$  to minimize  $\mathbb{E}_u[(D_{\mathcal{X}}(u) - 1)^2]$  and train the  $D_{\mathcal{X}}$  to minimize  $\mathbb{E}_u[D_{\mathcal{X}}(u)^2] + \mathbb{E}_x[(D_{\mathcal{X}}(x) - 1)^2]$ . We can also formulate  $\mathcal{L}_{adv}^y$  symmetrically. For convenience, we define:

$$\mathcal{L}_{adv}^{domain} = \mathcal{L}_{adv}^x + \mathcal{L}_{adv}^y \quad (7)$$

We repeat the encoding and generation operations again on the generated images. Finally, we get  $x' = G_{\mathcal{X}}(E_{\mathcal{Y}}^c(v), E_{\mathcal{X}}^s(u))$  and  $y' = G_{\mathcal{Y}}(E_{\mathcal{X}}^c(u), E_{\mathcal{Y}}^s(v))$ , which should be identical to the original ones, such as  $x$  or  $y$ . Inspired by [24, 42], we use cross-cycle-consistency loss to enforce this constraint. This loss could be formulated as:

$$\mathcal{L}_{cc} = \mathbb{E}_x\|x' - x\|_1 + \mathbb{E}_y\|y' - y\|_1 \quad (8)$$

### 3.3. Objective Function

We also use other loss functions to improve our framework.

**Self-reconstruction loss.** When  $x$  is encoded to content feature and style feature, the generator  $G_{\mathcal{X}}$  should recover  $x$ . Let denote  $\hat{x} = G_{\mathcal{X}}(E_{\mathcal{X}}^c(x), E_{\mathcal{X}}^s(x))$  and  $\hat{x}$  should be identical to  $x$ , we formulate this constrain as  $\mathcal{L}_{recon}^x = \mathbb{E}_x\|\hat{x} - x\|_1$ . We also formulate  $\mathcal{L}_{recon}^y$  symmetrically. Self-reconstruction loss ensures that we have exacted all information we need. The self-reconstruction loss could be formulated as follows totally:

$$\mathcal{L}_{recon} = \mathcal{L}_{recon}^x + \mathcal{L}_{recon}^y \quad (9)$$

**Latent regression loss.** Similar to BicycleGAN [43], we add latent regression loss to encourage invertible mapping between the real images and fake images. Latent regression loss also avoids posterior collapse of style encode and

prevent generator from ignoring style information [4]. We minimize the following loss:

$$\mathcal{L}_{latent} = \mathbb{E}_x \|z - E_{\mathcal{X}}^s(G_{\mathcal{X}}(z, E_{\mathcal{X}}^c(x)))\|_1 + \mathbb{E}_y \|z - E_{\mathcal{Y}}^s(G_{\mathcal{Y}}(z, E_{\mathcal{Y}}^c(y)))\|_1 \quad (10)$$

where  $z$  is sampled from gaussian distribution  $\mathcal{N}(0, I)$ .

**Total objection function.** Totally, the full objective function of our method is as follows:

$$\begin{aligned} \mathcal{L} = & \lambda_{cc} \mathcal{L}_{cc} + \lambda_{recon} \mathcal{L}_{recon} + \lambda_{adv}^c \mathcal{L}_{adv}^c \\ & + \lambda_{adv}^{domain} \mathcal{L}_{adv}^{domain} + \lambda_{seg} \mathcal{L}_{seg} + \lambda_{adv}^f \mathcal{L}_{adv}^f \\ & + \lambda_{KL} \mathcal{L}_{KL} + \lambda_{latent} \mathcal{L}_{latent} \end{aligned} \quad (11)$$

where the hyper parameter  $\lambda$  controls the importance of each term. In practice, we set  $\lambda_{cc} = \lambda_{recon} = \lambda_{latent} = 10$ ,  $\lambda_{adv}^c = \lambda_{adv}^{domain} = \lambda_{seg} = \lambda_{adv}^f = 1$  and  $\lambda_{KL} = 0.01$ .

At test time, images from target domain are forwarded into content encoder  $E_{\mathcal{Y}}^c$  and segmentation module  $S_{seg}$ . In this way, we can obtain segmentation results  $\tilde{y} = S_{seg}(E_{\mathcal{Y}}^c(y))$ .

### 3.4. Implement details

In this section, we describe the network architecture of proposed method. We implemented our framework in PyTorch 1.8.1 on a RTX 2080Ti GPU. For content encoder, we use an architecture consisting of 6 convolution layers with an instance normalization layer and 8 residual blocks [17]. For style encoder, we use a CNN architecture with 5 convolution layers and full connected layers. The style encode is set to  $s \in R^8$ . For generator, we use 3 residual blocks and 3 nearest-neighbor upsampling layers to get the same resolution with input images. We share the weight between the last 3 layers of  $E_{\mathcal{X}}^c$  and  $E_{\mathcal{Y}}^c$  and the first layers of  $G_{\mathcal{X}}$  and  $G_{\mathcal{Y}}$ . For segmentation network  $S_{seg}$ , we use 4 residual blocks and 3 upsampling layers to get segmentation result. For all discriminators, we follow the configuration of PatchGAN proposed in [20]. For training, we used the Adam optimizer with a batch size of 4 and with a learning rate of 0.001 for segmentation network and 0.0001 for other networks. We keep the same learning rate for the first 150 epochs and linearly decay the learning rate to zero over the next 150 epochs. More details could be found in our supplement materials.

## 4. Experiments and Results

### 4.1. Datasets and Preprocessing

We evaluated our method on two public datasets. The first dataset is MR-CT dataset<sup>1</sup>, an open dataset mainly from Multi-Modality Whole Heart Segmentation Challenge [38, 46]. The dataset includes 52 CT images and 46 MR

images from different subjects. Only 20 subjects of dataset have gold standard segmentation for MR or CT data. We use 10 subjects of them for test and other images are used for training. We exact 16 slices for every subject from long-axis view around the heart to train our model. The second dataset<sup>2</sup> is from Multi-sequence Cardiac MR Segmentation (MSCMR) Challenge (MICCAI 2019) [44, 45], which contains three sequences cardiac MR images from 45 subjects. We use two sequence images from each subjects: bSSFP and LGE images. 25 LGE and 45 bSSFP images are used for training and 20 LGE images are used for evaluation. Note that the LGE and bSSFP images are collected from the same patient, so we shuffle the dataset to make them unpaired.

For all datasets, we resample images to  $1 \times 1$  mm slice by slice and crop them to  $192 \times 192$ . We convert images to  $[-1, 1]$  before feeding into the network. The data augmentations include rotation and flipping.

### 4.2. Experiment Details and Evaluation Metrics

We trained our model from scratch and evaluated our method on two datasets as mentioned. For MR-CT dataset, we evaluated our method in two directions, *i.e.* setting CT as source domain and MR as target domains and setting MR as source domain and CT as target domain in turn. For MSCMR dataset, we only evaluate on one direction, *i.e.* bSSFP images as source domain and LGE images as target domain. We aim to segment the myocardium of left ventricle (MYO), left ventricular cavity (LV), and right ventricular cavity (RV) for two datasets.

For evaluation, we used two commonly-used metrics for medical image segmentation: Dice coefficient ([%]) and average symmetric surface distance (ASSD). Dice coefficient measures overlap between prediction and ground truth and ASSD evaluates the segmentation performance at object boundary. We evaluated our method slice by slice on both MR-CT dataset and MSMCR dataset. Note that higher Dice coefficient and lower ASSD mean better performance.

### 4.3. Performance and Comparison

We compare our method with some popular unsupervised domain adaptations methods.

- Unet(supervised) [31]: We trained a unet model with labeled targeted data. This result could be upper bound for unsupervised domain adaptation. Note that this is a strong baseline for our experiments.
- Unet(no adaptation) [31]: We trained a Unet model with labeled source data and directly test on the target data without any domain adaptation.

<sup>1</sup>[https://github.com/FupingWu90/CT\\_MR\\_2D\\_Dataset\\_DA](https://github.com/FupingWu90/CT_MR_2D_Dataset_DA)

<sup>2</sup><http://www.sdspeople.fudan.edu.cn/zhuangxiahai/0/mscmrseg19/>

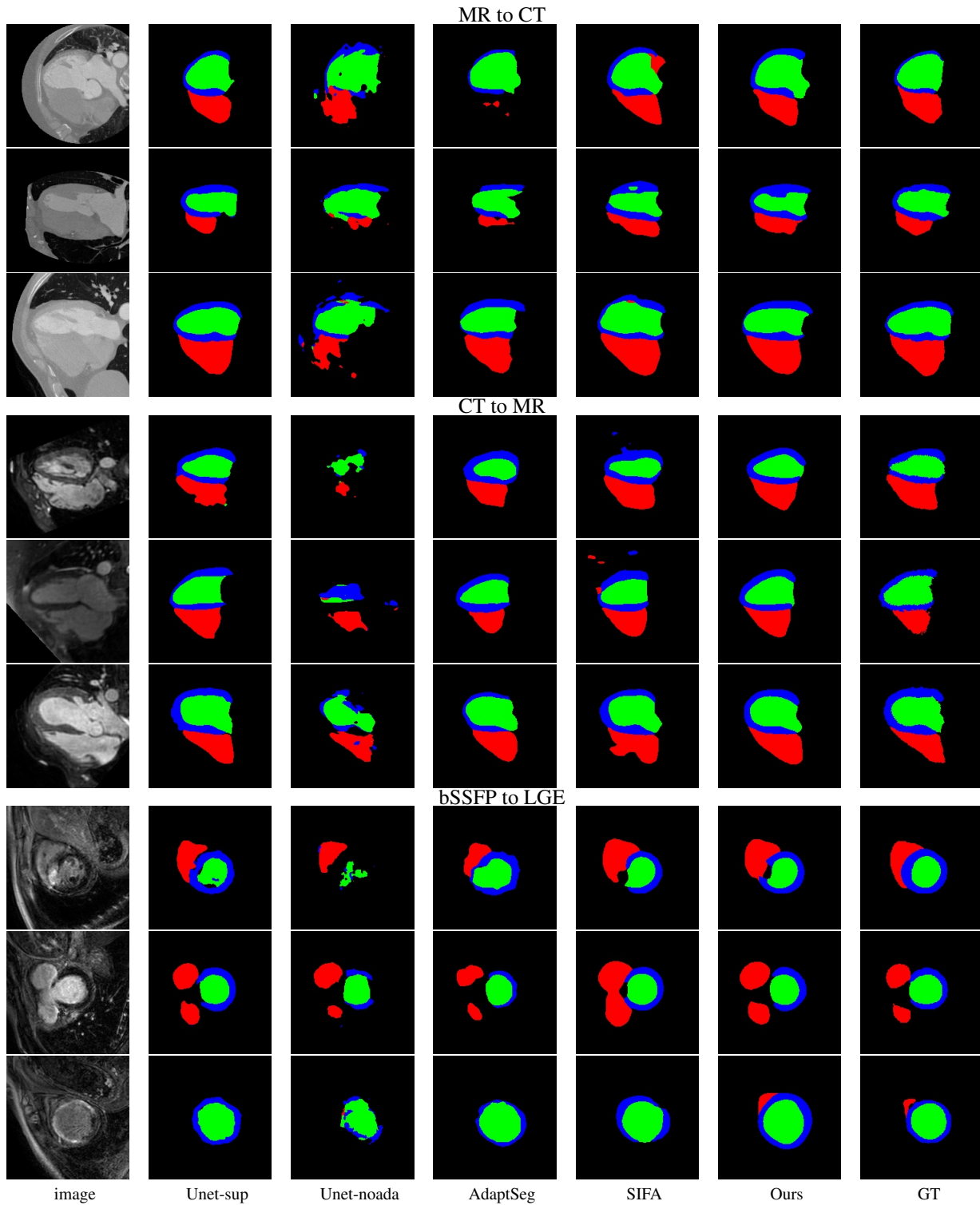


Figure 4. Visual comparison of segmentation results of different methods. The structures MYO, LV and RV are indicated in blue, green and red respectively. From left to right: raw data sampled from target domain (1st column), results of different compared models (from 2nd column to 4th column), our results (5th column), ground truth of raw data (last column).

Table 1. Performance comparison between our model and other unsupervised domain adaptation methods on three tasks. We evaluate performance from two metrics: Dice and ASSD for all cardiac structure and average. Note that higher Dice and lower ASSD mean better performance.

MR → CT								
Method	Dice(%)				ASSD(mm)			
	MYO	LV	RV	Average	MYO	LV	RV	Average
Unet(supervised) [31]	86.89	93.04	90.75	90.27	1.24	1.33	1.85	1.47
Unet(no adaptation) [31]	29.88	74.87	51.99	52.24	6.54	5.96	8.55	7.02
AdaptSeg [34]	47.65	77.41	64.43	63.16	3.78	3.41	5.18	4.12
SIFA [5]	52.94	82.32	83.62	72.96	3.19	3.88	4.00	3.69
Ours	69.26	85.86	85.42	80.18	2.36	2.69	3.70	2.58
CT → MR								
Method	Dice(%)				ASSD(mm)			
	MYO	LV	RV	Average	MYO	LV	RV	Average
Unet(supervised) [31]	82.84	93.86	90.81	89.17	1.46	1.69	1.93	1.69
Unet(no adaptation) [31]	14.84	53.67	62.13	43.55	10.85	8.88	6.69	8.80
AdaptSeg [34]	47.80	74.30	73.30	62.13	4.80	4.66	4.33	4.59
SIFA [5]	65.30	78.60	76.00	73.30	5.20	4.60	6.20	5.30
Ours	65.42	83.66	79.20	76.10	3.55	4.17	4.66	4.12
bSSFP → LGE								
Method	Dice(%)				ASSD(mm)			
	MYO	LV	RV	Average	MYO	LV	RV	Average
Unet(supervised) [31]	77.46	86.49	70.91	78.29	1.67	1.52	2.37	1.85
Unet(no adaptation) [31]	33.77	62.03	48.96	48.25	5.26	4.69	6.29	5.41
AdaptSeg [34]	47.02	69.03	66.71	60.92	2.95	3.00	3.80	3.25
SIFA [5]	63.63	77.57	61.58	67.59	2.50	3.00	3.76	3.09
Ours	68.29	82.56	64.00	71.61	2.00	2.43	4.27	2.90

- AdaptSeg [34]: This is one of the state of the art methods for unsupervised domain adaptation. AdaptSeg aligned data for source domain and target domain on feature level. For a fair comparison, we also used pre-trained model of Deeplabv2-ResNet101 on ImageNet [11] in experiments, the same as original paper.
- SIFA [5]: SIFA is one of the state of the art unsupervised domain adaptation methods for medical image segmentation. Different from AdaptSeg, SIFA aligned data on images levels and feature levels.

We reimplement all methods with the original public author’s code and apply directly with default configurations in original paper. Note that we referenced our model as SGDR for simplicity, the acronym for Semantic-guided Disentangled representation. We present quantitative results in Tab. 1 and the visual comparisons are shown in Fig. 4.

It could be seen that our method has a significant improvement compared to Unet without domain adaptation from Tab. 1, which has 28%, 23%, 22% higher Dice than comparison methods on three tasks, respectively. More importantly, our model also outperforms the current state of

the art methods on three tasks, especially SIFA [5]. Our model has a 7.22%, 2.8%, 3% higher dice score than SIFA and 1.11, 1.18, 0.19 lower ASSD values than SIFA, respectively. The quantitative results demonstrate the effectiveness of our model.

Fig. 4 shows the visual results of all comparison methods. We show the results of three cases of all the compared methods in three tasks. It is observed that Unet [31] trained on source domain without any domain adaptation can hardly predict the cardiac structure correctly. By using some domain adaptation methods, such as AdaptSeg [34] (4th column) or SIFA [5] (5th column) can recover segmentation prediction partly, but there are still some wrong predictions and unclear boundaries. Specially, our results are closer to the ground truth and less wrong predictions than other methods, which shows that our model is more robust and accurate.

#### 4.4. Ablation Study

Our proposed method uses semantic-guided strategy to improve the performance. In the section, we study the effectiveness of content discriminator, feature discriminator

Table 2. Evaluate the effectiveness of three components of our method on MR-CT task. 'w/o' means remove this component from our implement. We report average Dice score of ablation study.

Method	Average Dice(%)
No adaptation	52.24
SGDR w/o content discriminator	69.6
SGDR w/o feature discriminator	72.4
SGDR w/o loss $\mathcal{L}_{seg}^v$	77.8
SGDR	80.18

and loss  $\mathcal{L}_{seg}^v$  on MR-CT task. The quantitative results are reported in Tab. 2, where 'w/o' means to remove the module from our implements. First, the content discriminator encourages encoders to capture domain-invariant features by adversarial training, which improve the performance of domain adaptation by a large margin. Second, we use adversarial training in the semantic space between target images and synthetic target images. We remove the feature discriminator from our model in ablation study. The results show that the feature discriminator can effectively increase average Dice from 72.4% to 80.18%. Finally, we evaluated the effectiveness of loss  $\mathcal{L}_{seg}^v$ . In this work, we use two segmentation loss,  $\mathcal{L}_{seg}^x$  and  $\mathcal{L}_{seg}^v$ . The loss function  $\mathcal{L}_{seg}^v$  could further constrain the encoder to exact the anatomical structure of source domain more accurately and get 2.38% improvement. Overall, the ablation study shows that the semantic-guided strategy of our model achieves better performance and contributes to improvement jointly.

## 5. Conclusion

We present a novel semantic-guided disentangled representation model for unsupervised domain adaptation of cross-modality medical image segmentation. Our model uses semantic-guided strategy to exact the meaningful domain-invariant features for segmentation task. We apply a content discriminator to help encoders exact domain-invariant features and a feature discriminator to exact the meaningful representation of source domain and target domain. Moreover, an auxiliary segmentation loss is used to keep the anatomical structure and help us exact more meaningful information. We evaluated our method on two public datasets and the experiment results show that our framework improves the performance of segmentation task in target domain by a large margin. Our model can also be readily extended to 3D medical image segmentation task in unsupervised domain adaptation setting, although our work is demonstrated on 2D data.

## References

[1] Sagie Benaim, Michael Khaitov, Tomer Galanti, and Lior Wolf. Domain intersection and domain difference. In

*Proceedings of the IEEE/CVF International Conference on Computer Vision*, pages 3445–3453, 2019.

[2] Konstantinos Bousmalis, George Trigeorgis, Nathan Silberman, Dilip Krishnan, and Dumitru Erhan. Domain separation networks. *Advances in neural information processing systems*, 29:343–351, 2016.

[3] Dawood Al Chanti and Diana Mateus. Olva: Optimal latent vector alignment for unsupervised domain adaptation in medical image segmentation. In *International Conference on Medical Image Computing and Computer-Assisted Intervention*, pages 261–271. Springer, 2021.

[4] Agisilaos Chatsias, Giorgos Papanastasiou, Chengjia Wang, Scott Semple, David E Newby, Rohan Dharmakumar, and Sotirios A Tsaftaris. Disentangle, align and fuse for multimodal and semi-supervised image segmentation. *IEEE transactions on medical imaging*, 40(3):781–792, 2020.

[5] Cheng Chen, Qi Dou, Hao Chen, Jing Qin, and Pheng-Ann Heng. Synergistic image and feature adaptation: Towards cross-modality domain adaptation for medical image segmentation. In *Proceedings of the AAAI Conference on Artificial Intelligence*, volume 33, pages 865–872, 2019.

[6] Cheng Chen, Qi Dou, Yueming Jin, Hao Chen, Jing Qin, and Pheng-Ann Heng. Robust multimodal brain tumor segmentation via feature disentanglement and gated fusion. In *International Conference on Medical Image Computing and Computer-Assisted Intervention*, pages 447–456. Springer, 2019.

[7] Chen Chen, Cheng Ouyang, Giacomo Tarroni, Jo Schlemper, Huaqi Qiu, Wenjia Bai, and Daniel Rueckert. Unsupervised multi-modal style transfer for cardiac mr segmentation. In *International Workshop on Statistical Atlases and Computational Models of the Heart*, pages 209–219. Springer, 2019.

[8] Xi Chen, Yan Duan, Rein Houthoofd, John Schulman, Ilya Sutskever, and Pieter Abbeel. Infogan: Interpretable representation learning by information maximizing generative adversarial nets. In *Proceedings of the 30th International Conference on Neural Information Processing Systems*, pages 2180–2188, 2016.

[9] Eleni Chiou, Francesco Giganti, Shonit Punwani, Iasonas Kokkinos, and Eleftheria Panagiotaki. Harnessing uncertainty in domain adaptation for mri prostate lesion segmentation. In *International Conference on Medical Image Computing and Computer-Assisted Intervention*, pages 510–520. Springer, 2020.

[10] Nicolas Courty, Rémi Flamary, Amaury Habrard, and Alain Rakotomamonjy. Joint distribution optimal transportation for domain adaptation. In *Proceedings of the 31st International Conference on Neural Information Processing Systems*, pages 3733–3742, 2017.

[11] Jia Deng, Wei Dong, Richard Socher, Li-Jia Li, Kai Li, and Li Fei-Fei. Imagenet: A large-scale hierarchical image database. In *2009 IEEE conference on computer vision and pattern recognition*, pages 248–255, 2009.

[12] Qi Dou, Cheng Ouyang, Cheng Chen, Hao Chen, and Pheng-Ann Heng. Unsupervised cross-modality domain adaptation of convnets for biomedical image segmentations with adversarial loss. In *Proceedings of the 27th International Joint Conference on Artificial Intelligence*, pages 691–697, 2018.



- [13] Andre Esteva, Alexandre Robicquet, Bharath Ramsundar, Volodymyr Kuleshov, Mark DePristo, Katherine Chou, Claire Cui, Greg Corrado, Sebastian Thrun, and Jeff Dean. A guide to deep learning in healthcare. *Nature medicine*, 25(1):24–29, 2019.
- [14] Yaroslav Ganin, Evgeniya Ustinova, Hana Ajakan, Pascal Germain, Hugo Larochelle, François Laviolette, Mario Marchand, and Victor Lempitsky. Domain-adversarial training of neural networks. *The journal of machine learning research*, 17(1):2096–2030, 2016.
- [15] Abel Gonzalez-Garcia, Joost van de Weijer, and Yoshua Bengio. Image-to-image translation for cross-domain disentanglement. In *NeurIPS*, 2018.
- [16] Ian Goodfellow, Jean Pouget-Abadie, Mehdi Mirza, Bing Xu, David Warde-Farley, Sherjil Ozair, Aaron Courville, and Yoshua Bengio. Generative adversarial nets. *Advances in neural information processing systems*, 27, 2014.
- [17] Kaifeng He, Xiangyu Zhang, Shaoqing Ren, and Jian Sun. Deep residual learning for image recognition. In *Proceedings of the IEEE conference on computer vision and pattern recognition*, pages 770–778, 2016.
- [18] Xun Huang, Ming-Yu Liu, Serge Belongie, and Jan Kautz. Multimodal unsupervised image-to-image translation. In *Proceedings of the European conference on computer vision (ECCV)*, pages 172–189, 2018.
- [19] Fabian Isensee, Paul F Jaeger, Simon AA Kohl, Jens Petersen, and Klaus H Maier-Hein. nnu-net: a self-configuring method for deep learning-based biomedical image segmentation. *Nature methods*, 18(2):203–211, 2021.
- [20] Phillip Isola, Jun-Yan Zhu, Tinghui Zhou, and Alexei A Efros. Image-to-image translation with conditional adversarial networks. In *Proceedings of the IEEE conference on computer vision and pattern recognition*, pages 1125–1134, 2017.
- [21] Jue Jiang and Harini Veeraraghavan. Unified cross-modality feature disentangler for unsupervised multi-domain mri abdomen organs segmentation. In *International Conference on Medical Image Computing and Computer-Assisted Intervention*, pages 347–358. Springer, 2020.
- [22] Konstantinos Kamnitsas, Christian Baumgartner, Christian Ledig, Virginia Newcombe, Joanna Simpson, Andrew Kane, David Menon, Aditya Nori, Antonio Criminisi, Daniel Rueckert, et al. Unsupervised domain adaptation in brain lesion segmentation with adversarial networks. In *International conference on information processing in medical imaging*, pages 597–609. Springer, 2017.
- [23] Guoliang Kang, Yunchao Wei, Yi Yang, Yueting Zhuang, and Alexander Hauptmann. Pixel-level cycle association: A new perspective for domain adaptive semantic segmentation. *Advances in Neural Information Processing Systems*, 33, 2020.
- [24] Hsin-Ying Lee, Hung-Yu Tseng, Jia-Bin Huang, Maneesh Singh, and Ming-Hsuan Yang. Diverse image-to-image translation via disentangled representations. In *Proceedings of the European conference on computer vision (ECCV)*, pages 35–51, 2018.
- [25] Kang Li, Lequan Yu, Shujun Wang, and Pheng-Ann Heng. Towards cross-modality medical image segmentation with online mutual knowledge distillation. In *Proceedings of the AAAI Conference on Artificial Intelligence*, volume 34, pages 775–783, 2020.
- [26] Xiaomeng Li, Hao Chen, Xiaojuan Qi, Qi Dou, Chi-Wing Fu, and Pheng-Ann Heng. H-denseunet: hybrid densely connected unet for liver and tumor segmentation from ct volumes. *IEEE transactions on medical imaging*, 37(12):2663–2674, 2018.
- [27] Mingsheng Long, Yue Cao, Jianmin Wang, and Michael Jordan. Learning transferable features with deep adaptation networks. In *International conference on machine learning*, pages 97–105. PMLR, 2015.
- [28] Xudong Mao, Qing Li, Haoran Xie, Raymond YK Lau, Zhen Wang, and Stephen Paul Smolley. Least squares generative adversarial networks. In *Proceedings of the IEEE international conference on computer vision*, pages 2794–2802, 2017.
- [29] Munan Ning, Cheng Bian, Dong Wei, Shuang Yu, Chenglang Yuan, Yaohua Wang, Yang Guo, Kai Ma, and Yefeng Zheng. A new bidirectional unsupervised domain adaptation segmentation framework. In *International Conference on Information Processing in Medical Imaging*, pages 492–503. Springer, 2021.
- [30] Chenhao Pei, Fuping Wu, Liqin Huang, and Xiahai Zhuang. Disentangle domain features for cross-modality cardiac image segmentation. *Medical Image Analysis*, 71:102078, 2021.
- [31] Olaf Ronneberger, Philipp Fischer, and Thomas Brox. U-net: Convolutional networks for biomedical image segmentation. In *International Conference on Medical image computing and computer-assisted intervention*, pages 234–241. Springer, 2015.
- [32] Zhao Shi, Chongchang Miao, U Joseph Schoepf, Rock H Savage, Danielle M Dargis, Chengwei Pan, Xue Chai, Xiu Li Li, Shuang Xia, Xin Zhang, et al. A clinically applicable deep-learning model for detecting intracranial aneurysm in computed tomography angiography images. *Nature communications*, 11(1):1–11, 2020.
- [33] Baochen Sun and Kate Saenko. Deep coral: Correlation alignment for deep domain adaptation. In *European conference on computer vision*, pages 443–450. Springer, 2016.
- [34] Yi-Hsuan Tsai, Wei-Chih Hung, Samuel Schuster, Kihyuk Sohn, Ming-Hsuan Yang, and Manmohan Chandraker. Learning to adapt structured output space for semantic segmentation. In *Proceedings of the IEEE conference on computer vision and pattern recognition*, pages 7472–7481, 2018.
- [35] Eric Tzeng, Judy Hoffman, Kate Saenko, and Trevor Darrell. Adversarial discriminative domain adaptation. In *Proceedings of the IEEE conference on computer vision and pattern recognition*, pages 7167–7176, 2017.
- [36] Eric Tzeng, Judy Hoffman, Ning Zhang, Kate Saenko, and Trevor Darrell. Deep domain confusion: Maximizing for domain invariance. *arXiv preprint arXiv:1412.3474*, 2014.
- [37] Daiju Ueda, Akira Yamamoto, Masataka Nishimori, Taro Shimono, Satoshi Doishita, Akitoshi Shimazaki, Yutaka Katayama, Shinya Fukumoto, Antoine Choppin, Yuki

- Shimahara, et al. Deep learning for mr angiography: automated detection of cerebral aneurysms. *Radiology*, 290(1):187–194, 2019.
- [38] Fuping Wu and Xiahai Zhuang. CF distance: A new domain discrepancy metric and application to explicit domain adaptation for cross-modality cardiac image segmentation. *IEEE Transactions on Medical Imaging*, 39(12):4274–4285, 2020.
- [39] Fuping Wu and Xiahai Zhuang. Unsupervised domain adaptation with variational approximation for cardiac segmentation. *IEEE Transactions on Medical Imaging*, 2021.
- [40] Junlin Yang, Nicha C Dvornek, Fan Zhang, Julius Chapiro, MingDe Lin, and James S Duncan. Unsupervised domain adaptation via disentangled representations: Application to cross-modality liver segmentation. In *International Conference on Medical Image Computing and Computer-Assisted Intervention*, pages 255–263. Springer, 2019.
- [41] Yefeng Zheng, David Liu, Bogdan Georgescu, Hien Nguyen, and Dorin Comaniciu. 3d deep learning for efficient and robust landmark detection in volumetric data. In *International conference on medical image computing and computer-assisted intervention*, pages 565–572. Springer, 2015.
- [42] Jun-Yan Zhu, Taesung Park, Phillip Isola, and Alexei A Efros. Unpaired image-to-image translation using cycle-consistent adversarial networks. In *Proceedings of the IEEE international conference on computer vision*, pages 2223–2232, 2017.
- [43] Jun-Yan Zhu, Richard Zhang, Deepak Pathak, Trevor Darrell, Alexei A Efros, Oliver Wang, and Eli Shechtman. Toward multimodal image-to-image translation. In *Advances in Neural Information Processing Systems*, 2017.
- [44] Xiahai Zhuang. Multivariate mixture model for cardiac segmentation from multi-sequence mri. In *International Conference on Medical Image Computing and Computer-Assisted Intervention*, pages 581–588. Springer, 2016.
- [45] Xiahai Zhuang. Multivariate mixture model for myocardial segmentation combining multi-source images. *IEEE transactions on pattern analysis and machine intelligence*, 41(12):2933–2946, 2018.
- [46] Xiahai Zhuang and Juan Shen. Multi-scale patch and multi-modality atlases for whole heart segmentation of mri. *Medical Image Analysis*, pages 77–87, 2016.